Redox Biology 64 (2023) 102763

Contents lists available at ScienceDirect

Redox Biology

journal homepage: www.elsevier.com/locate/redox

NOX2 inhibition stabilizes vulnerable plaques by enhancing macrophage efferocytosis via MertK/PI3K/AKT pathway

Yue Wang, Xin-yan Liu, Yue Wang, Wen-xin Zhao, Fa-dong Li, Peng-rong Guo, Qian Fan, Xiao-fan Wu *

Department of Cardiology, Beijing Anzhen Hospital, Capital Medical University, Beijing, China

ARTICLE INFO

Keywords:
Atherosclerosis
Vulnerable plaque
NOX2
Efferocytosis
Mertk

ABSTRACT

NADPH oxidases 2 (NOX2) is the main source of ROS in macrophages, which plays a critical role in the formation of atherosclerosis. However, effects of NOX2 inhibition on established vulnerable plaques and the potential role involved remain unclear. The purpose of this study is to investigate the latent mechanism of NOX2-triggered vulnerable plaque development. We generated a vulnerable carotid plaque model induced by carotid branch ligation and renal artery constriction, combined with a high-fat diet in ApoE$^{-/-}$ mice. NOX2 specific inhibitor, GSK2795039 (10 mg/kg/day by intragastric administration for 8 weeks) significantly prevented vulnerable plaque, evaluated by micro-ultrasound imaging parameters. A profile of less intraplaque hemorrhage detection, increased collagen-lipid ratio, fibrous cap thickness and less necrotic core formation were also found in GSK2795039 treated group. Mechanistically, reduced 4-HNE, in situ lesional apoptosis and enhanced efferocytosis were involved in mice treated with NOX2 inhibitor. Further analysis in mouse macrophages confirmed the role of NOX2 inhibition in enhancing macrophage efferocytosis by regulating the MertK/PI3K/AKT pathway. In summary, our data defined previously few recognized roles of NOX2 in vulnerable plaque pathogenesis and an undescribed NOX2-ROS-MerTK axis acts involved in regulating macrophage efferocytosis in the formation of rupture-prone vulnerable plaques.

1. Introduction

Myocardial infarctions and ischaemic strokes, which complicate atherosclerosis arise from thrombosis or formation of blood clots, have been the leading causes of death worldwide. Most acute thromboses are provoked by a physical disruption of atherosclerotic plaques. Therefore, more and more attention has been paid to the so-called "vulnerable plaque" [1].

One of the most characteristic hallmarks of vulnerable plaque is the necrotic core, which is caused by impaired removal of apoptotic cells (AC) in the diseased blood vessel [2]. Macrophages recognize and internalize oxidized low-density lipoproteins (ox-LDL) to eventually become lipid-laden foam cells which eventually to be dead. Efferocytosis refers to the phagocytic engulfment of a cellular corpse. Tabas et al. concluded in their review that the problem during vulnerable plaque formation is not the consequence of too much cell death but rather too little cell clearance [3]. Further, the apoptotic cells facilitate the necrotic core formation and promoting the interaction among the components in the plaque, such as oxidative stress and nonresolving inflammation response. However, the crucial factors regulating the efficiency of efferocytosis and oxidative stress are not fully elucidated.

Oxidative stress is one of the major mediators of the secondary injury during atherothrombosis. Though the reactive oxygen species (ROS) can be produced from many sources in macrophages, NADPH oxidases 2 (NOX2), also called gp91phox, is the main source of ROS in macrophages which is the member of the only family of enzymes solely devoted to the production of ROS. NOX2 inhibition has been shown to cause regression of vascularization and the size and stability of atherosclerotic plaques [4]. But whether there exists any crosstalk between NOX2 and efferocytosis, and the consequences of this crosstalk in mediating plaque vulnerability has not been known.

In this study, we explored the impacts of NOX2 inhibition on vulnerable plaques, using a mouse model of rupture-prone plaques, and the role of NOX2 inhibition on the efficiency of macrophage efferocytosis *in vitro/in vivo*. Furthermore, we conducted mechanistic studies to elucidate the mechanism by which NOX2-medicated ROS regulated

* Corresponding author. Department of Cardiology, Beijing Anzhen Hospital, Capital Medical University , 2 Anzhen Rd, Chaoyang District , Beijing, 100029, China.
E-mail address: drwuxf@163.com (X.-f. Wu).

https://doi.org/10.1016/j.redox.2023.102763
Received 8 May 2023; Received in revised form 21 May 2023; Accepted 24 May 2023
Available online 17 June 2023

the efferocytosis. These efforts may enlarge our knowledge of the crosstalk between NOX2 and efferocytosis in vulnerable plaque from a therapeutic perspective.

2. Materials and methods

2.1. Experimental animals

Animal protocols were approved by the Animal Care and Use Committee of Capital Medical University, and the study was performed according to the National Institutes of Health Guide for the Care and Use of Laboratory Animals.

8-week-old male ApoE$^{-/-}$ mice on a C57BL/6 background (SPF Biotechnology, Beijing, China) were randomly enrolled into 2 groups: vehicle and GSK2795039. All the mice received surgery in which the branch ligation of the left common carotid artery (LCCA) was performed, and the left renal artery was constricted. In brief, as previously described [5,6], mice were anesthetized with isoflurane via inhalation through a nose mask and were maintained through-out the surgery at 37 °C on a heating pad. First, the anterior cervical triangles were accessed by a sagittal anterior neck incision. The LCCA was individualized from circumferential connective tissues by blunt dissection and the exposed branches of the LCCA but not the superior thyroid artery was permanently ligated with a surgical suture. Next, after a small flank incision the left kidney was exposed, and the left renal artery was ligated with a surgical suture along with a pin gauge (0.12 mm in diameter) to preserve renal perfusion (Supplementary Fig. 1). After the surgery, the GSK2795039 and vehicle groups were administered GSK2795039 (HY-18950, MedChem Express, 10 mg/kg per day) and the solvent (composed with 10% DMSO, 40% PEG300, 5% Tween-80 and 45% saline), respectively, for 8 weeks by intragastric administration. All the mice were fed with a high-fat diet (0.15% cholesterol and 21% fat, 4 kcal/g) during the 8-week experiment.

2.2. Ultrasound imaging

Ultrasound imaging parameters of left common carotid artery were measured using the Vevo770 system (Visual Sonics, Canada.) 4 weeks and 8 weeks after surgery. In brief, mice were anesthetized with inhaled 2% isoflurane (Lunan Pharmaceutical Group, China), neck hair was defoliated, and echo gel liberally applied. A 30-MHz scan head was applied to measure lumen diameters in M-mode, extreme values of intimal-medial thickness (IMT) in M-mode, and center stream peak-systolic (Vmax) and time-averaged velocities were evaluated in pulse wave Doppler mode [7]. The eccentric index (EI) was calculated from the extreme values of IMT using the formula (maximal IMT − minimal IMT)/maximal IMT to measure the degree of eccentric plaque distribution [8].

2.3. Tissue acquisition

Mice were anesthetized with 1% pentobarbital sodium (i.p. 60 mg/kg) followed by cardiac puncture to collect blood which were placed in centrifuge tubes containing heparin (10 μl, 1000 IU mL −1). After centrifugation at 3000 rpm for 15 min at 4 °C, the plasma was collected and stored at −80 °C for further analysis. Then, after removed the connected and fat tissues, the common carotid arteries were individualized under a microscope, then a gross picture was taken by a camera. The left common carotid artery was harvested and stored in 4% paraformaldehyde for further use or frozen in optimal cutting temperature (OCT) embedding compound (Sakura, Netherlands) and stored at −80 °C.

2.4. Histological staining of left common carotid artery in ApoE$^{-/-}$ mice

6-μm cryosections of left common carotid arteries embedded in OCT and 5-μm cryosections of left common carotid arteries embedded in paraffin were taken using Leica for hematoxylin and eosin and Masson's trichrome staining. 7-μm cryosections of left common carotid arteries embedded in OCT were captured into sections for Oil red O staining.

2.5. Immunofluorescence and immunohistochemistry

Paraffin-embedded specimens were sectioned, deparaffinized with xylene, and rehydrated in decreasing concentrations of ethanol. After washing with PBS, slides were incubated in 5% BSA for 30 min, stained with the specific primary antibody (CD68, ab53444, Abcam, 1:200; MerTK, ab300136, Abcam, 1:200; anti-Phospho-AKT (Ser473) Monoclonal antibody, 66444-1-Ig, proteintech, 1:200; α-SMA antibody, ab7817, Abcam, 1:200; 4-Hydroxynonenal antibody, ab48506, Abcam, 1:200) overnight [9], then stained with the corresponding secondary antibody and counterstained with DAPI (4′,6-diamidino-2-phenylindole) or hematoxylin. Images were captured using a fluorescence microscope (fluorescence microscope BX41, Olympus, Japan).

2.6. In situ lesional apoptosis and efferocytosis assay

Lesional apoptosis and in situ efferocytosis were visualized by immunofluorescent staining with TUNEL staining reagents (11684817910, Roche) and anti- CD68 (ab53444, 1:200, Abcam) antibody. Sections were incubated with TUNEL staining reagents at room temperature for 60 min and then washed three times with PBS. Sections were then blocked with 5% BSA for 60 min, incubated overnight at 4 °C with an anti-CD68 antibody. At last, slides were incubated with fluorescently labeled secondary antibodies and counterstained with DAPI.

As a measure of defective efferocytosis, we counted the number of free versus macrophage-associated apoptotic cells in individual lesional sections [7]. Free apoptotic cells were defined as TUNEL + cells that exhibited nuclear condensation, loss of antibody CD68 reactivity, and were not in contact with neighboring macrophages. Macrophage-associated apoptotic cells were defined as cells with TUNEL + nuclei surrounded by or in contact with neighboring CD68^{+} macrophages [10–12]. All analysis was performed by 2 independent assessors blinded to the experiment details.

2.7. Determination of malonaldehyde, superoxide dismutase and ox-LDL levels

The levels of malonaldehyde (MDA), superoxide dismutase (SOD) and ox-LDL in mouse serum were measured using MDA assay kit (A003-1, Nanjing Jiancheng Bioengineering Institute, China), SOD assay kit (A001-1, Nanjing Jiancheng Bioengineering Institute, China) and Mouse ox-LDL ELISA Kit (JYM0050Mo, Colorful-Gene Biotech, China) according to the manufacturer's instructions.

2.8. Primary mouse macrophage and neutrophil isolation and culture

For bone marrow-derived macrophages (BMDM), mice were sacrificed and both femurs and tibias were dissected and flushed with sterile 1X PBS, which was passed through a 100 μM cell strainer and collected. The cells were spun down (1000×*g*, 5 min), washed with 1X PBS, and plated in RPMI (supplemented with 10% FBS, 1% Pen-strep) with M-CSF (10 ng/mL). Cells were allowed to differentiate into macrophages for 5 days after which media was changed daily for further use [13].

Peripheral blood neutrophils were obtained by first spinning heparinized blood on Histopaque-1083 (Sigma-Aldrich, USA) according to the manufacturer's instructions. Remaining red blood cells were lysed with RBC Lysis Buffer (multi-species) according to the manufacturer's instructions (R1010, Solarbio, China), and the remaining neutrophils were washed with PBS before use. Cells had the typical segmented nuclei of mature neutrophils by microscopy [14,15].

2.9. Cell culture and foam cell formation

The mouse monocyte/macrophage cell line, RAW264.7 (ATCC, USA) was cultured in RPMI 1640 media supplemented with 10% heat inactivated FBS, 100 U/mL penicillin, and 100 mg/mL streptomycin at 37 °C in a humidified incubator with a 5% CO2 atmosphere.

RAW264.7 or BMDM differentiated with M-CSF were plated on 12 mm glass coverslips with 0.2% gelatin. Cells were cultured in RPMI (serum free) supplemented with 1% Pen-strep for 24 h and then treated with 50 μg/mL oxLDL (YB-002, Yiyuan Biotechnologies, China) for 24 h to establish foam cell model [16]. Cells were fixed in 4% PFA for 20 min at room temperature and washed with PBS. For Oil Red O staining, coverslips were stained with Oil Red O, washed with PBS, counterstained with hematoxylin, washed with PBS. (Supplementary Fig. 2).

2.10. Stable transfection

RAW264.7 cells were transfected with pLVX-mNox2-3flag-ZsGreen-Puro (NM_007807.5) plasmid, control vector, and pLVX-shRNA-Puro-mNox2 (GeneID:13058) (control shRNA vector) plasmid followed by 5ug/ml puromycin selection and stable clones were maintained in 5 μg/ml concentration. Successful overexpression and knockdown were confirmed by Western blot assessments of NOX2 protein levels (Table S1 and Supplementary Fig. 3). All the infections were at multiplicities of infection (MOI) of 50.

2.11. In vitro efferocytosis assay

Jurkat (human T-lymphocyte) cells (ATCC, USA) were maintained in RPMI 1640 media supplemented with 15% heat-inactivated FBS, 100 U/mL penicillin, and 100 mg/mL streptomycin at 37 °C in a humidified incubator with a 5% CO2 atmosphere. Apoptosis of Jurkat cells was induced by UV exposure (30 mJ/cm^2, 75min), followed by incubation for 3.6 h (37 °C, 5% CO_2 atmosphere), a time sufficient to generate late apoptosis [17]. As detected by dual annexin V/PI staining and flow cytometry, more than 70% of the Jurkat population were annexin-positive and PI-positive. Then the Jurkat cells were co-cultured with macrophages at a 1:5 ratio for 90 min at 37 °C. After co-culture, non-engulfed Jurkat cells were extensively washed with cold PBS. Efferocytosis was quantified by flow cytometry utilizing a previously described method [18] with a BD LSRFortessa and associated software (BD FACS Diva Software). The results were expressed as efferocytosis index, defined as the percentage of macrophages that engulfed apoptotic cells relative to the total number of macrophages.

2.12. ROS measurement

The intracellular ROS levels were determined using 2′,7′-dichlorofluorescin diacetate (DCFH-DA, S0033, Beyotime Biotechnology, China) and dihydroethidium (DHE, S0063, Beyotime Biotechnology, China). Macrophages cultured in a 6-well plate were incubated in the dark with 10 μM DCFH-DA or DHE at 37 °C for 30 min before being trypsinized, washed, and resuspended in 0.5 mL of PBS for flow cytometry analysis. FlowJo software (BD Biosciences, New York, NY, USA) was used to analyze the results.

2.13. Flow cytometry analysis

Apoptosis assays were performed by exposing cultured Jurkat cells to UV light as above described, then staining them by Annexin V-fluorescein (FITC)/propidium iodide (PI) double-staining assay (556547, Becton, Dickinson and Company, NJ, USA). Cells were stained with annexin V-FITC and PI on ice for 20 min in the dark. Then the single-cell suspension was filtered, centrifuged, and resuspended in PBS. The percentage of Jurkat apoptosis was analyzed by flow cytometry (BD LSRFortessa) and associated software (BD FACSDiva Software) (Supplementary Fig. 4).

Efferocytosis assays of RAW264.7 and BMDM were performed by incubating macrophages with CellTrackerTM Deep Red (C34565, Invitrogen, CA, USA) and incubating apoptotic cells with Vybrant® CFDA SE Cell Tracer Kit (V12883, Invitrogen, CA, USA). Efferocytosis assays of transfected RAW264.7 were performed by incubating macrophages with Vybrant® CFDA SE Cell Tracer Kit (V12883, Invitrogen, CA, USA) and incubating apoptotic cells with CellTrackerTM Deep Red (C34565, Invitrogen, CA, USA). Events were acquired on flow cytometry (BD LSRFortessa) with more than 10,000 cells per group, and results were analyzed on FlowJo (BD Biosciences, NY, USA). The results were expressed as efferocytosis index, defined as the percentage of macrophages that engulfed apoptotic Jurkats relative to the total number of macrophages (relative to the control group) [17,19].

2.14. Reverse transcription polymerase chain reaction

RNA was isolated from RAW264.7 cells with Trizol reagent (Invitrogen, USA). The purity of RNA was assessed by absorbance at 260 and 280 nm using the NanoDrop spectrophotometer (Thermo Scientific, USA) and then reverse transcribed using 1 μg of the total RNA to generate cDNA (RR047A, Takara, Japan). Quantitative real-time polymerase chain reaction (PCR) was performed with SYBR Green Master Mix (RR820A, Takara, Japan) with primers using a LightCycler® 480 System (Roche, Germany). Samples were amplified for 40 cycles (5 s at 95 °C, 30 s at 60 °C) after an initial enzyme activation for 30 s at 95 °C. The last cycle was followed by 10 s at 95 °C and 5 s at 65 °C. All samples were analyzed in triplicate and were normalized to GAPDH. The $2^{-\Delta\Delta Ct}$ method was used to analyze the relative changes in gene expression. PCR primers used in this study are listed in Table S2.

2.15. Western blotting analysis

Cells were lysed in complete lysis-M (Roche, Germany) plus the protease and phosphatase inhibitor (Thermo Scientific, USA) containing 1% β-Mercaptoethanol and heated at 100 °C for 10 min. Protein concentration of samples prepared from RAW264.7 cells were evaluated by utilizing the BCA Protein Assay Kit (23227, Thermo, MA, USA). 30–50 μg of protein per sample was separated via gel electrophoresis, transferred to a poly-vinylidene fluoride membrane, and blocked with 5% milk for 1 h. The membrane was incubated overnight with primary antibodies at 4 °C. After incubation with the Dye 800-conjugated anti-mouse antibody (1:10,000, 926-32210, LI-COR Biosciences, Lincoln, USA) or anti-rabbit antibody (1:10,000, 926-32211, LI-COR Biosciences, Lincoln, USA), the images were visualized and analyzed using Odyssey infrared imaging system (LI-COR Biosciences, Lincoln, USA).

The primary antibodies used in this study were: anti-gp91phox (1:1000,sc130543, Santa Cruz), anti-MERTK (phospho Y749) + TYRO3 (phospho Y681) antibody (1:1000, ab192649, abcam), anti-MERTK antibody (1:1000, ab300136, abcam), anti-Phospho-PI3 Kinase p85 (Tyr458)/p55 (Tyr199) antibody (1:1000, #4228, CST), anti-PI3 Kinase antibody (1:1000, #4257, CST), anti-AKT antibody (1:1000, 10176-2-AP, proteintech), anti-Phospho-AKT (Ser473) Monoclonal antibody (1:1000, 66444-1-Ig, proteintech), anti-GAPDH antibody (1:1000, 60004-1-Ig, proteintech).

2.16. Statistical analysis

All results in this study are presented as mean ± SEM. Data were analyzed with GraphPad Prism (Version 7.0, CA, USA). Student *t*-test was used to assess the effects of parameters between 2 different groups (unpaired test). $P < 0.05$ was considered as being statistically significant.

3. Results

3.1. NOX2 inhibition reduces vulnerable features in ApoE$^{-/-}$ mice

To explore the effect of NOX2 inhibition on vulnerable plaque instability, the mouse model of rupture-prone vulnerable carotid plaques was established at 4 weeks after surgery (Supplementary Fig. 1). In the model, GSK2795039, a specific NOX2 inhibitor, and its vehicle were administered to ApoE$^{-/-}$ mice for 56 days, and micro-ultrasound scans of left carotid arteries were taken at day 28 and day 56 (Fig. 1A). At day 28, there is no statistically difference in carotid IMT, EI, maximal systolic velocity and blood flow between GSK2795039 and vehicle group. After another 4-week treatment, the plaques from GSK2795039-treated ApoE$^{-/-}$ mice showed decreased IMT, EI, maximal systolic velocity and increased blood flow (Fig. 1B), a lower carotid plaque burden, lipid burden compared with those from vehicle-treated ApoE$^{-/-}$ mice (Fig. 1C). The collagen-lipid ratio and fibrous cap thickness, which are reliable indicators of plaque stability, were also significantly increased in GSK2795039-treated ApoE$^{-/-}$ mice (Fig. 1C). These data suggested that NOX2 inhibition stabilizes rupture-prone vulnerable plaques.

3.2. NOX2 inhibition enhanced macrophage efferocytosis in carotid vulnerable plaques

Macrophage efferocytosis has been recognized as an important step to remove the apoptotic cells, which facilitate the necrotic core formation and plaque rupture. To detect apoptosis and efferocytosis in plaque areas and investigate whether NOX2 was involved in these processes, sections of carotid plaques were co-stained for DNA fragmentation with TUNEL staining and macrophage surface marker with CD68 antibody (Fig. 2A). Compared with the vehicle group, the relative number of lesional free apoptotic cells decreased on GSK2795039 intervention (Fig. 2A). Meanwhile, macrophage-associated apoptotic cells, which underwent efferocytosis, increased in plaque areas of GSK2795039 group (Fig. 2A), suggesting that NOX2 might play a role in the defective macrophage efferocytosis in carotid vulnerable plaques.

3.3. NOX2 deficiency improves macrophage efferocytosis in response to ox-LDL in vitro

To further explore the role and potential mechanism of NOX2 in regulating efferocytosis, we did subsequent experiments focusing on macrophage efferocytosis in *vitro*. Model of foam cell was first established by pre-exposing RAW264.7 or BMDM cells to 50 μg/ml ox-LDL for 24 h as previously mentioned. Then, in line with animal experiments, macrophages were first incubated with 50 μM GSK2795039 for 12 h before incubating with apoptotic cells. We found GSK2795039 also increased efferocytosis both in RAW264.7 and in BMDM cells (Fig. 2B–D). Next, we generated a shRNA to mouse NOX2, which was able to achieve significant knockdown of NOX2 in RAW264.7 cells. Of note, the efferocytosis index was also significantly increased by NOX2 knockdown, consistent with previous results (Fig. 2E). Together, these data indicate that, consistent with GSK2795039 treatment in *vivo*, NOX2 knockdown improved efferocytosis in *vitro*.

3.4. NOX2 induces defective macrophage efferocytosis through regulating ROS

We further investigated whether ROS decrease mediated the beneficial effects of NOX2 inhibition against vulnerable plaque rupture. First, we demonstrated the functional validity of NOX2 inhibitor in *vivo*. We detected ROS in the carotid plaques using 4-HNE immunostaining and determined the serum biochemistry, oxLDL, MDA and SOD concentration. We found that GSK2795039 treatment resulted in a remarkable decrease of 4-HNE positive area in the plaque, decrease of serum oxLDL, decrease of serum MDA, and increase of serum SOD in mice (Fig. 3A).

Then we detected ROS and efferocytosis by flow cytometry in *vitro*. It showed that GSK2795039 treatment could decrease the level of ROS both in RAW264.7 and BMDM cells (Fig. 3B and C). NOX2 knockdown could also decrease the level of ROS, consistent with previous results (Fig. 3D). Next, we generated NOX2 overexpression RAW264.7 cells (Supplementary Fig. 3) with increased ROS. Treatment with 10 nM N-Acetyl-L-cysteine (NAC), which is ROS scavenger, could alleviate defective macrophage efferocytosis induced by NOX2 overexpression, accompanying with decreased ROS (Fig. 3E and F). These data indicated that ROS is the medium of NOX2 inducing defective macrophage efferocytosis.

However, in addition to macrophages, NOX2 is also highly expressed in neutrophils, which is also get defective due to high ROS production and contributes to the increased mass of vulnerable plaques [20–22]. To demonstrate the effect of ROS decrease on macrophage efferocytosis is not disturbed by ROS decrease of neutrophils, we induced neutrophil apoptosis and treated them with vehicle or 50 μM GSK2795039. BMDMs in Vehicle and GSK2795039 group were then co-incubated with apoptotic neutrophils respectively. It is found that when NOX2 was inhibited in neutrophils, GSK2795039 can still enhance efferocytosis of BMDMs (Fig. 3G). These data indicate that the systemic effects seen in ApoE$^{-/-}$ mice can be owing to macrophage-specific inhibition of NOX2 despite GSK2795039 also inhibited NOX2 in other cell types.

3.5. Deletion of NOX2 upregulates MerTK expression to improve macrophage efferocytosis

Since the process of efferocytosis can be mainly divided into three parts: apoptotic cell finding, apoptotic cell binding, apoptotic cell internalization and degradation. To clarify the underlying mechanism of NOX2 inhibition on promoted efferocytosis, we focused on the well-known important macrophage-associated signal during these processes, including MerTK, SRBI, LRP1, growth arrest-specific protein 6 (Gas6) and milk fat globule-eGF factor 8 (Mfge8), taking part in binding molecules on the apoptotic cell surface or binding bridging molecules that interact with the apoptotic cell surface [2,23]. After NOX2 knockdown or overexpression in RAW264.7, we performed RT-PCR to evaluate the mRNA expression of MerTK, SRBI, LRP1, Gas6 and Mfge8 and found that MerTK was most affected by NOX2 (Fig. 4A). Furthermore, using western blotting, we confirmed the increased expression of phospho-MerTK combining with NOX2 knockdown in RAW264.7 (Fig. 4B) and NOX2 inhibition in BMDMs (Fig. 4C). The decreased expression of phospho-MerTK was also found after NOX2 over-expression. ROS scavenger, NAC, could also prevented the inactivation of MerTK induced by NOX2 over-expression (Fig. 4D). Meanwhile, inhibiting the phosphorylation of MerTK with UNC2025, the protecting role of NOX2 knockdown in the efferocytosis of RAW264.7 faded (Fig. 4E).

Furthermore, we verified the effects of NOX2 inhibition on macrophage MerTK in *vivo*. Increased MerTK expression of macrophages was observed in the carotid plaques of ApoE$^{-/-}$ mice treated with GSK2795039 (Fig. 4F). Overall, these results indicate that NOX2 inhibition decreases ROS, increases MerTK expression and finally promotes efferocytosis.

3.6. Deletion of NOX2 in macrophages enhanced efferocytosis via the PI3K/AKT pathway

The PI3K/AKT pathway has been identified as a critical regulatory factor in macrophage efferocytosis, and the phosphorylation of PI3K and AKT is one of the several downstream signaling pathways of MerTK activation [24,25]. Thus, we further investigated the effects of NOX2 on PI3K/AKT phosphorylation/activation in macrophages. GSK2795039 significantly promoted PI3K/AKT phosphorylation in BMDMs (Fig. 5A). Sh NOX2 significantly promoted PI3K/AKT phosphorylation (Fig. 5B) and NOX2 over-expression decreased the activation of PI3K/AKT

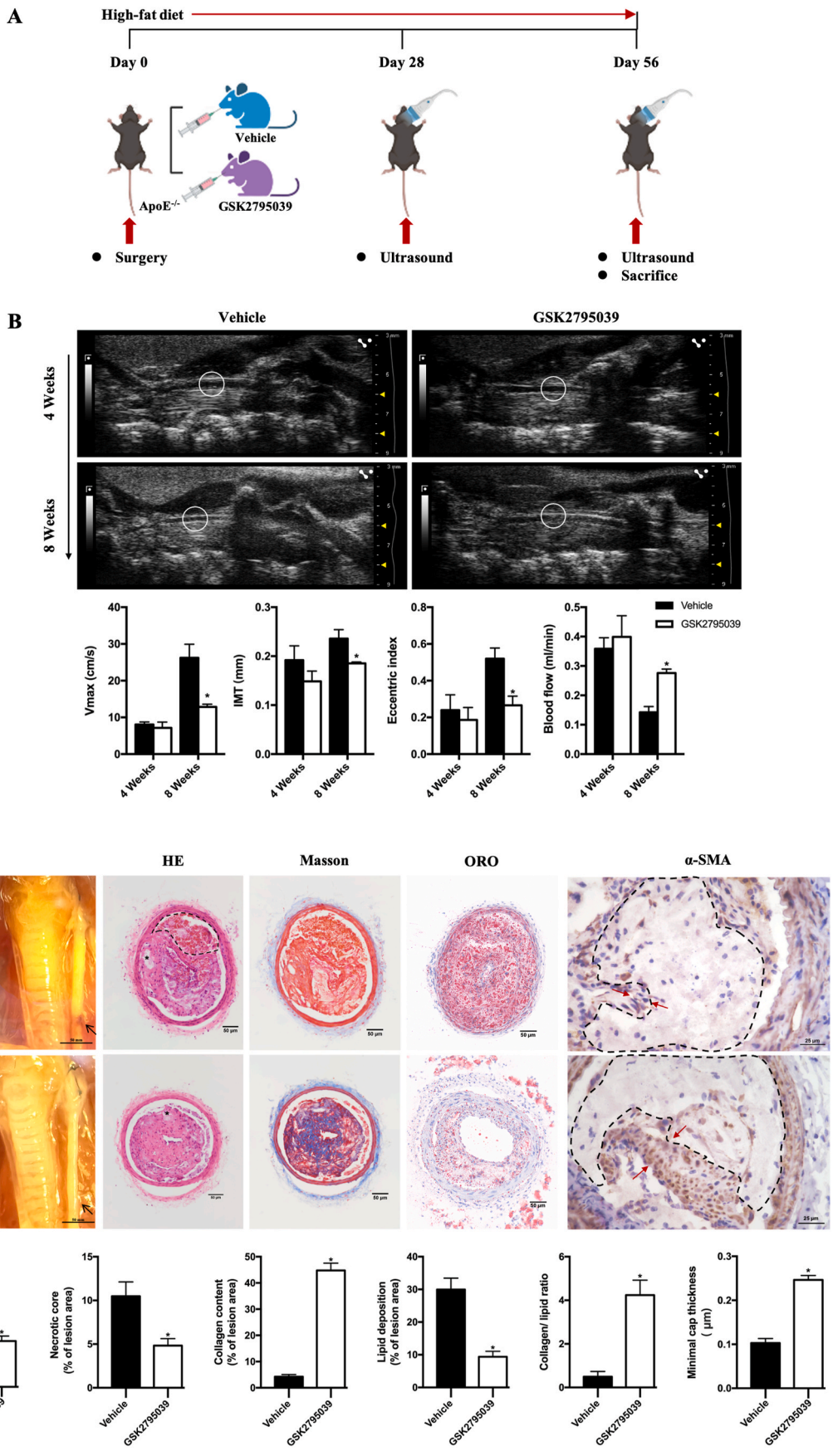

(caption on next page)

Fig. 1. NOX2 inhibition reduces vulnerable features in ApoE$^{-/-}$ mice.
A. Schematic protocol: ApoE$^{-/-}$ mice received surgery to establish the model of rupture-prone vulnerable carotid plaques and were intragastric administrated with Vehicle or GSK2795039 (a specific NOX2 inhibitor, 10 mg/kg per day) for 8 weeks (n = 10 per group). Micro-ultrasound images were obtained at day 28 and 56. **B.** Long-axis views of the left common carotid arterial segments by micro-ultrasound 4 weeks and 8 weeks after surgery. Ultrasound-derived maximal systolic velocity (Vmax), ultrasound-derived plaque intimal-medial thickness (IMT), eccentric index (EI) and blood flow were quantified in the vehicle- and GSK2795039-treated ApoE$^{-/-}$ mice. n = 6 per group. *P < 0.05 versus Vehicle. **C.** Representative photomicrographs of the left common carotid arterial segments at 8 weeks after surgery. Representative carotid artery cross-sections were stained with HE, Masson, Oil red O and α-SMA staining. In HE staining, dashed lines encircle intraplaque hemorrhage and the asterisks indicate necrotic cores. Quantification of the atherosclerotic lesion area, necrotic core area, plaque collagen and lipid content were displayed in the corresponding histogram. Plaque stability was assessed by the collagen-to-lipid ratio and minimal cap thickness. Minimal cap thickness was measured at the thinnest region of the fibrotic cap (indicated by the red arrows in α-SMA staining) surrounding the necrotic core (encircled by the dashed lines) in α-SMA staining. n = 6 per group. *P < 0.05 versus Vehicle. (For interpretation of the references to colour in this figure legend, the reader is referred to the Web version of this article.)

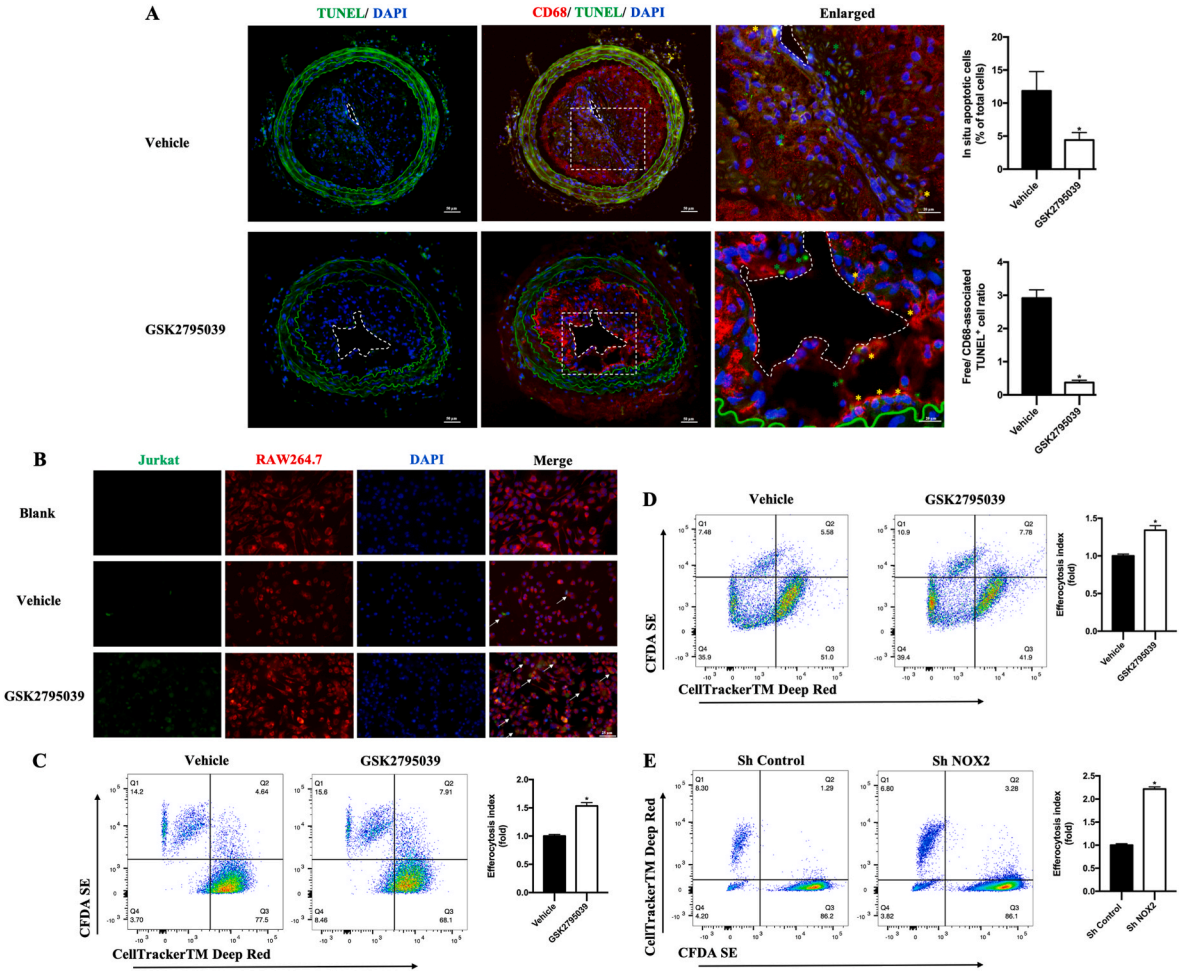

Fig. 2. NOX2 inhibition enhanced macrophage efferocytosis in *vivo* and in *vitro*.
A. Representative immunofluorescence staining of apoptosis and efferocytosis in carotid sections. Apoptotic cells were stained with TUNEL (green) and macrophages were stained with an anti-CD68 antibody (red). Dashed lines encircle the lumen in the first column of A. Dotted squares (the second column in A) indicate the corresponding part of the enlarged pictures (the third column in A). In the third column, yellow asterisks show examples of macrophage-associated apoptotic cells, whereas green asterisks indicate free apoptotic cells. Quantification of lesional apoptotic cells (percentage of total cells) and quantification of lesional efferocytosis index were shown in the histograms. The efferocytosis index is the free apoptotic cells/macrophage-associated apoptotic cells. n = 6 per group. *P < 0.05 versus Vehicle. **B.** Representative probe staining of efferocytosis in RAW264.7. Macrophage labeled by CellTrackerTM Deep Red (red) was cocultured with CFDA SE (green) labeled apoptotic Jurkat. Arrows in the fourth column of B indicates efferocytosis - macrophages with engulfed apoptotic Jurkats. **C.** Representative flow cytograms of efferocytosis in Vehicle and GSK2795039 group, with RAW264.7 labeled with CellTrackerTM Deep Red and Jurkats labeled with CFDA SE. Quantification of efferocytosis index in RAW264.7. The efferocytosis index is the double positive cells (Q2)/macrophage cells (Q2+ Q3) and relative to the Vehicle. n = 6 per group. *P < 0.05 versus Vehicle. **D.** Representative flow cytograms of efferocytosis in Vehicle and GSK2795039 group, with BMDM labeled with CellTrackerTM Deep Red and apoptotic cells labeled with CFDA SE. Quantification of efferocytosis index in BMDM. The efferocytosis index is the double positive cells (Q2)/macrophage cells (Q2+ Q3) and relative to the Vehicle. n = 6 per group. *P < 0.05 versus Vehicle. **E.** Representative flow cytograms of efferocytosis in Sh Control and Sh NOX2 group, with RAW264.7 labeled with CFDA SE and Jurkats labeled with CellTrackerTM Deep Red. Quantification of efferocytosis index. The efferocytosis index is the double positive cells (Q2)/macrophage cells (Q2+ Q3) and relative to the Sh Control. n = 6 per group. *P < 0.05 versus Sh Control. (For interpretation of the references to colour in this figure legend, the reader is referred to the Web version of this article.)

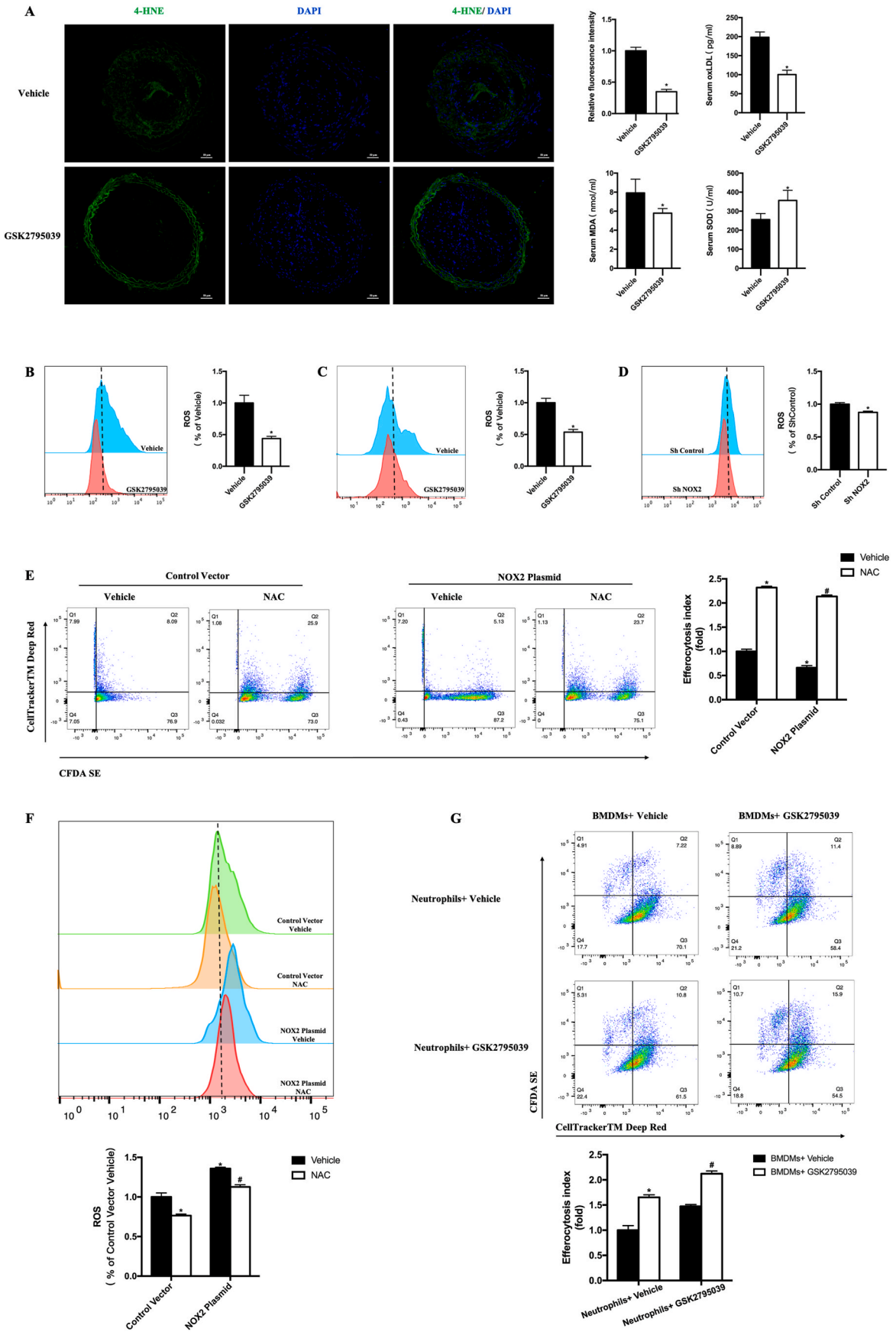

(caption on next page)

Fig. 3. NOX2 induces defective macrophage efferocytosis through regulating ROS.
A. Representative immunofluorescence staining of 4-HNE in mouse carotid sections. Quantification of fluorescence intensity of 4-HNE in mouse carotid plaque. Quantification of oxLDL, MDA and SOD concentration in mouse serum. n = 6 per group. *P < 0.05 versus Vehicle. **B.** Representative flow cytograms of ROS level with DCFH-DA staining of RAW264.7. Quantification of ROS relative to Vehicle. **C.** Representative flow cytograms of ROS level with DCFH-DA staining of BMDMs. Quantification of ROS relative to Vehicle. n = 6 per group. *P < 0.05 versus Vehicle. **D.** Representative flow cytograms of ROS level with DHE staining in group of Sh Control and Sh NOX2. Quantification of ROS relative to Sh Control. n = 6 per group. *P < 0.05 versus Sh Control. **E.** Representative flow cytograms of efferocytosis in RAW264.7 (treated with Control vector or NOX2 plasmid) with macrophages labeled with CFDA SE and Jurkats labeled with CellTrackerTM Deep Red. Quantification of efferocytosis index. The efferocytosis index is the double positive cells (Q2)/macrophage cells (Q2+Q3) and relative to the Control Vector Vehicle. n = 6 per group. *P < 0.05 versus Control Vector Vehicle. #P < 0.05 versus NOX2 Plasmid Vehicle. **F.** Representative flow cytograms of ROS level with DHE staining of RAW264.7. Quantification of ROS relative to Control Vector Vehicle. n = 6 per group. *P < 0.05 versus Control Vector Vehicle. #P < 0.05 versus NOX2 Plasmid Vehicle. **G.** Representative flow cytograms of efferocytosis in BMDMs with macrophages labeled with CellTrackerTM Deep Red and neutrophils labeled with CFDA SE. Neutrophils were treated with vehicle or 50 μM GSK2795039 for 12 h. Then apoptosis of neutrophils was induced by UV exposure (30 mJ/cm^2, 75min), followed by incubation for 3.6 h (37 °C, 5% CO_2 atmosphere), a time sufficient to generate late apoptosis. Finally, apoptotic neutrophils were co-cultured with BMDMs. Quantification of efferocytosis index. The efferocytosis index is the double positive cells (Q2)/macrophage cells (Q2+Q3) and relative to the neutrophil Vehicle and BMDM Vehicle. n = 6 per group. *P < 0.05 versus neutrophil Vehicle and BMDM Vehicle. #P < 0.05 versus neutrophil GSK2795039 and BMDM Vehicle. (For interpretation of the references to colour in this figure legend, the reader is referred to the Web version of this article.)

(Fig. 5C). Exposing macrophages to UNC2025, a novel MerTK-selective small-molecule tyrosine kinase inhibitor, significantly reduced PI3K/AKT activation, which indicates PI3K/AKT activation being MerTK-mediated downstream signaling (Fig. 5B). Then to clarify the role of ROS as a medium in NOX2 regulating efferocytosis, the effect of NAC treatment on PI3K/AKT activation was explored in RAW264.7 with NOX2 overexpression. NAC treatment could alleviate decreased PI3K/AKT activation in NOX2 overexpressed macrophage (Fig. 5C).

Furthermore, we verified the effects of NOX2 inhibition on pAKT in *vivo*. Accordingly, increased pAKT expression was observed in the carotid plaques of ApoE$^{-/-}$ mice treated with GSK2795039 (Fig. 5D).

4. Discussion

Vulnerable plaques in atherosclerosis often cause acute cardiocerebral vascular events. It has been emphasized the need for a deeper understanding on the mechanism of vulnerable plaques and a new therapeutic strategy. Though the roles of NOX2 in atherosclerosis have been well established, whether there exists any crosstalk between NOX2 and efferocytosis, and the consequences of this crosstalk in mediating plaque vulnerability has not been known. In this study, we provided new insights into the regulatory role of NOX2-ROS-MerTK axis in the macrophage efferocytosis and demonstrated the therapeutic potential of NOX2 inhibition in stabilizing rupture-prone plaques (see the scheme in Fig. 6). We demonstrated that NOX2 inhibition alleviated vulnerable characteristics, such as lipid-rich plaque, intraplaque hemorrhage, a thin fibrous cap and necrotic core formation. Moreover, NOX2 inhibition stabilized rupture-prone plaques by facilitating efferocytosis of intraplaque macrophages through MerTK. Further analysis in mouse macrophage confirmed the role of NOX2-ROS-MerTK axis in regulating macrophage efferocytosis by regulating the PI3K/AKT pathway. In summary, our data provided novel evidence that NOX2 inhibition protects against vulnerable plaque rupture by regulating macrophage efferocytosis, of which MerTK is an important mediator.

NOX2 (also known as gp91phox or cytochrome *b*-245 heavy chain) was the first member of the NOX family to be discovered [26]. So far, it has also been recognized as the predominant source of ROS in atherosclerosis [27]. Roles of NOX2 in atherosclerosis have been investigated in genetically modified animal models on the background of ApoE$^{-/-}$, indicating that selective inhibition of NOX2 decreases aortic superoxide production and causes regression of vascularization and the size of atherosclerotic plaques [4,28,29]. However, the size of atherosclerotic plaques could not satisfied predict the risk of atherosclerotic plaques. It is of great importance to understand the mechanisms that induce plaque vulnerability [30,31]. Therefore, it is necessary to evaluate the ability of NOX2 inhibition to stabilize unstable plaques and prevent plaque rupture. In this study, we inhibited NOX2 with its novel small molecule inhibitor, GSK2795039, in a mouse model of rupture-prone vulnerable carotid plaques. GSK2795039 is the first small molecule identified that selectively inhibits NOX2 over other NOX isoforms in *vivo* [32,33]. Hirano K, et al. has proved that GSK2795039 inhibited both the formation of ROS and the utilization of the enzyme substrates, NADPH and oxygen [32]. It inhibited both NOX2 and ROS produced by NOX2 and was selective over other NOX isoforms, xanthine oxidase, and endothelial nitric oxide synthase enzymes. GSK2795039 showed activity in a murine model of acute pancreatitis, but it has been not used in atherosclerotic model yet [32]. Therefore, GSK2795039 is a good choice for this study to selectively inhibit NOX2 and explore the function of NOX2 inhibition. Here, we extended upon the established vasoprotective effects of NOX2 inhibition on atherosclerosis, by demonstrating that NOX2 inhibition stabilized vulnerable plaque by micro-ultrasound imaging and pathological staining.

Of note, endothelium-specific overexpression of NOX2 did not further accelerate the progression of atherosclerosis in ApoE$^{-/-}$ mice [34]. These results indicate that NOX2 has critical roles in atherosclerosis and cell type-specific contributions, except for endothelium, of NOX2-derived ROS warrant further investigation. Then we focused on the macrophages in the plaque, which play an important role during the process of oxidative stress. It is known that programmed cell death increased during atherosclerosis. But initially, macrophage has sufficient capacity to deal with this increase in apoptosis, which is so-called efferocytosis. Efferocytosis begins to fail in advanced plaques, leading to an accumulation of secondarily necrotic cells in an area of the plaque called the necrotic core [12,35]. Given macrophage both taking part in oxidative stress and efferocytosis, we suspect that NOX2 inhibition may affect macrophage efferocytosis and we indeed found that NOX2 inhibition alleviates defective efferocytosis in the carotid plaque by in situ lesional apoptosis and efferocytosis assay. Further, we conducted NOX2 gene knockdown and overexpression in cell line to validate its effect on efferocytosis. For the first time, we provide evidence that NOX2 inhibition promotes the stability of plaque by alleviating defective macrophage efferocytosis.

Though genetically modified hyperlipidemic mouse models have extensively been used to understand the mechanisms underlying the formation of atherosclerosis. These models only develop atherosclerosis and exhibit features similar to those of early human atherosclerosis and some features of advanced plaques [31]. The formation of necrotic core, intraplaque hemorrhage and plaque rupture are rarely observed in these genetically modified hyperlipidemic mouse models. Therefore, to explore the stability of atherosclerotic plaque, approaches to generate plaque de-stabilization based on surgical manipulation have been used in this study. The alteration of blood flow by performing the branch ligation of the LCCA induces local low shear stress in the carotid arteries and accelerates atherosclerosis and plaque vulnerability. Moreover, Jin SX, et al. proved that partly ligating the left renal artery can induce renovascular hypertension with endogenously increased angiotensin II production and accelerate plaque vulnerability [6]. Finally, at 4 weeks after surgery, the vulnerable plaque model was established and was

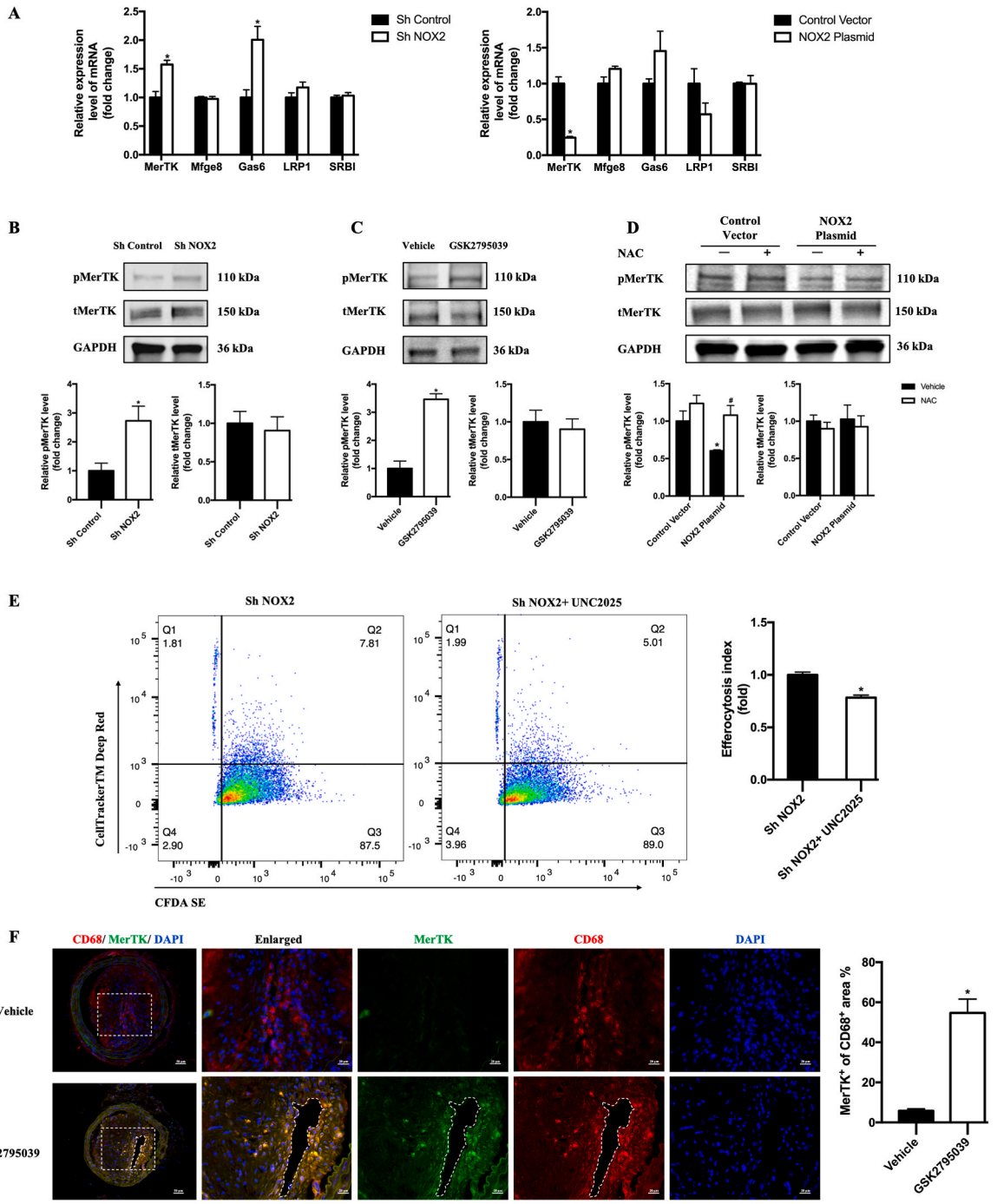

Fig. 4. NOX2 inhibition enhanced macrophage efferocytosis by regulating MerTK.
A. mRNA expression of MerTK, Mfge8, Gas6, SRB1 and LRP1 in RAW246.7 with NOX2 knockdown or overexpression. n = 6 per group, *P < 0.05 versus Sh Control or Control Vector. **B, C and D.** Western blotting was conducted on cell lysates with antibodies against p-MerTK, total MerTK (t-MerTK) and GAPDH. Relative densities of phosphorylated MerTK compared with total MerTK are shown as histograms. Relative densities of total MerTK compared with GAPDH are shown as histograms. n = 3 per group, *P < 0.05 versus Sh Control in B. *P < 0.05 versus Vehicle in C. *P < 0.05 versus Control Vector Vehicle in D, #P < 0.05 versus NOX2 Plasmid Vehicle in D. **E.** Representative flow cytograms of efferocytosis in Sh NOX2 RAW264.7 with macrophages labeled with CFDA SE and Jurkats labeled with CellTrackerTM Deep Red. Efferocytosis index was shown in the histograms. n = 6 per group, *P < 0.05 versus Sh NOX2. **F.** Representative photographs of carotid artery sections that were immunostained with CD68 antibodies (red) to label macrophages, and MerTK antibodies (green) to identify MerTK + macrophages. Quantification of the percentage of $MerTK^+$ cells in the $CD68^+$ area of arteries from GSK2795039-treated mice compared with that from vehicle-treated mice. n = 6 per group, *P < 0.05 versus Vehicle. (For interpretation of the references to colour in this figure legend, the reader is referred to the Web version of this article.)

verified by ultrasound imaging parameters.

To further explore the mechanism of NOX2 mediating macrophage efferocytosis, we first measured the level of ROS in macrophages with NOX2 knockdown and overexpression. Then we found that ROS scavenger NAC treatment, could alleviate defective macrophage efferocytosis induced by NOX2 overexpression. All these results linked ROS directly to the defects in efferocytosis. Since the process of efferocytosis involves several phases: AC finding, AC binding, AC internalization and AC degradation. AC finding is mainly regulated by chemokines released from AC to induce rapid mobilization of efferocytic

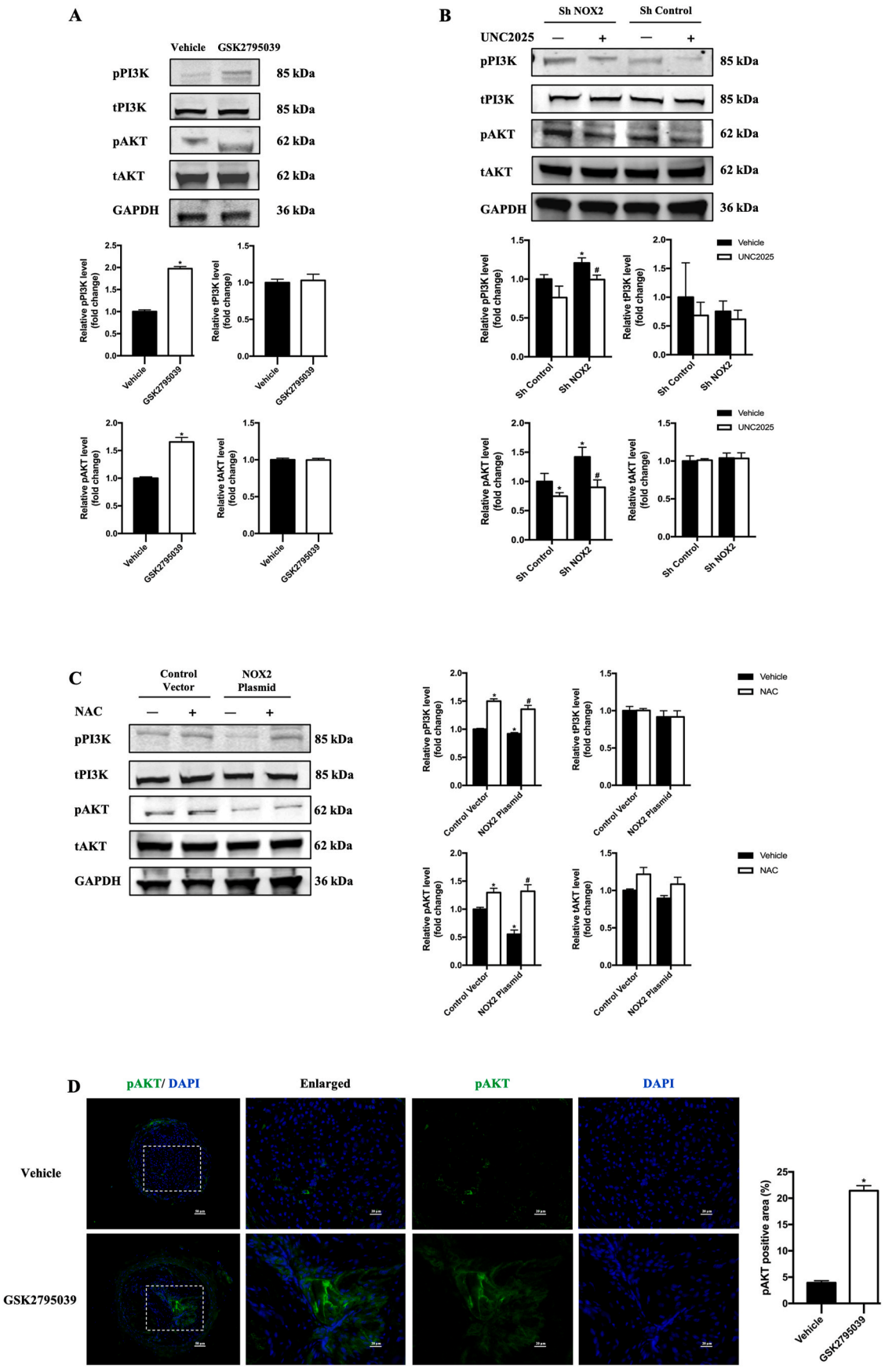

(caption on next page)

Fig. 5. Deletion of NOX2 in macrophages enhanced defective efferocytosis via the PI3K/AKT pathway
A, B and C. Western blotting was conducted on cell lysates with antibodies against p-PI3K, total PI3K (t- PI3K), p-AKT, total AKT (t- AKT), and GAPDH. Relative densities of phosphorylated PI3K compared with total PI3K are shown as histograms. Relative densities of phosphorylated AKT compared with total AKT are shown as histograms. Relative densities of total PI3K and total AKT compared with GAPDH are shown as histograms. n = 3 per group, *P < 0.05 versus Vehicle in A. *P < 0.05 versus Sh Control Vehicle in B. #P < 0.05 versus Sh NOX2 Vehicle in B. *P < 0.05 versus Control Vector Vehicle in C, #P < 0.05 versus NOX2 Plasmid Vehicle in C. The phosphorylated site of AKT was Ser473 and the phosphorylated site of PI3K was p85 (Tyr458). **D.** Representative photographs of carotid artery sections that were immunostained with pAKT antibodies (green). Quantification of pAKT positive area in the plaque. n = 6 per group, *P < 0.05 versus Vehicle. (For interpretation of the references to colour in this figure legend, the reader is referred to the Web version of this article.)

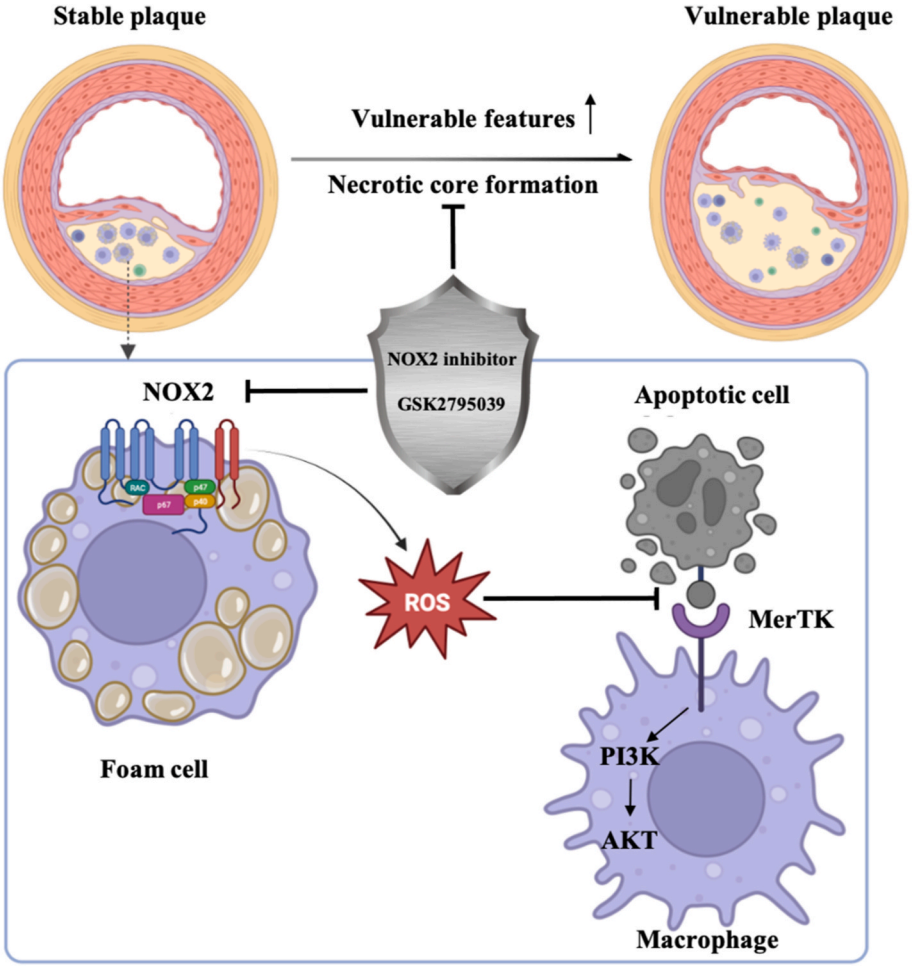

Fig. 6. The effect of NOX2 on efferocytosis and its inhibition stabilizes vulnerable plaque.
One of the most characteristic hallmarks of vulnerable plaque is the necrotic core, which is caused by impaired removal of apoptotic cells in the diseased blood vessel. Macrophages recognize and internalize ox-LDL to eventually become lipid-laden foam cells and NOX2 is inhibited to produce ROS. Excess ROS inhibits MerTK activation, which is an important macrophage receptor to facilitate binding apoptotic cells in efferocytosis. Finally, foam cells accumulate to promote lesion expansion, and apoptotic cells undergo secondary necrosis to accelerate lesion instability.

immune cells. Then, phagocytes engage AC through cell-surface receptors that either directly bind molecules on the AC surface or bind bridging molecules that interact with the AC surface. Finally, the ligation of efferocytosis receptor triggers intracellular signaling leading to Rac1 activation, actin polymerization, and AC engulfment [23,36,37]. AC binding is an important process bridging ACs and efferocytes [2], during which MerTK [38,39], LRP-1 [40], SR-B1 [24] and their bridging molecules, such as Gas6 [41], Mfge8 [42] have been suggested to have a role in atherosclerosis. So, the interaction between NOX2 and efferocytosis-related molecules need to be further explored.

MerTK, which has been shown expressing predominantly in phagocytic cells, has been identified a decreased macrophage expression in advanced plaques, and defective macrophage MerTK function impairs efferocytosis and promotes plaque necrosis [7,38]. After intervention of NOX2 expression, we also found that MerTK was affected by NOX2 in efferocytosis both in *vivo* and in *vitro*. Importantly, we provided evidence that loss of NOX2 increases efferocytosis and MerTK inhibitor reverses the protection of NOX2 inhibition in *vitro*, demonstrating a critical role for NOX2 inhibition in efferocytosis, which may be mediated by its impact on MerTK expression. Furthermore, inhibiting phosphorylation of MerTK with UNC2025, a novel MerTK-selective small-molecule tyrosine kinase inhibitor, reduced activation of MerTK-mediated downstream signaling, PI3K/AKT pathway [43,44], and impaired efferocytosis of macrophage. This supports a mechanism in which NOX2 inhibition promotes efferocytosis by activating MerTK and its downstream signaling to stabilize vulnerable plaques.

However, the present study has several limitations. First, in the study, we observed that NOX2 inhibition enhanced plaque stability and the interplay between NOX2 and macrophage efferocytosis. But the molecular basis of ROS-MerTK inter-connectivity remains to be addressed. Previous studies showed that the ectodomain of MerTK could be cleaved by the metalloproteinase ADAM17 [45,46]. This process disables MerTK, and the cleavage product, soluble Mer, would competitively inhibit the interaction of intact MerTK with its ligands which binds externalized phosphatidylserine on AC [47]. MerTK engagement triggers AC internalization via cytoskeletal signaling [48]. Whether these process, MerTK cleavage and cytoskeletal signaling, are regulated by NOX2 and ROS to interfere in efferocytosis needs further

investigation. Second, though NOXs are the predominant sources of ROS in cardiovascular system, different NOX isoforms have their specific effects on atherosclerosis. The role of other isoforms, NOX1 and NOX4 in efferocytosis still need to be further explored. Also, there are mainly three parts of efferocytosis: apoptotic cell finding, apoptotic cell binding, apoptotic cell internalization and degradation. This study explored NOX2 mediates MerTK which plays an important role in binding AC. Whether NOX2 takes part in the process of AC internalization and AC degradation still need to be further explored.

5. Conclusion

The present study unveils a previously unrecognized role of NOX2 in modulating macrophage efferocytosis in rupture-prone vulnerable plaques by mediating ROS and MerTK. In conclusion, the identification of NOX2 as a novel mediator regulating macrophage efferocytosis in vulnerable plaques might broaden our understanding of the therapeutic value of oxidative stress inhibition in stabilizing rupture-prone vulnerable plaques.

Author contributions

All authors contributed to the study conception and design. Yue Wang (the first author) performed experiments, analyzed and interpreted the data, and drafted the manuscript. Xin-yan Liu, Yue Wang (the third author), Wen-xin Zhao, Peng-rong Guo and Fa-dong Li conducted the experiments. Qian Fan analyzed and interpreted the data and edited the paper. Xiao-fan Wu contributed resources and secured funding, designed research, supervised the project and reviewed the manuscript.

Yue Wang (the first author) is a doctorial candidate of grade 2020; Yue Wang (the third author) is a postdoctoral fellow of grade 2022.

Ethics approval

All procedures involving animals were approved by the Capital Medical University Animal Experimentation Ethics Committee and carried out in accordance with the National Institutes of Health Guide for the Care and Use of Laboratory Animals.

Declaration of competing interest

Author declares no conflict of interest.

Data availability

Data will be made available on request.

Acknowledgments

This work was supported by the Beijing Natural Science Foundation and Municipal Education Commission Grant KZ202010025045, National Natural Science Foundation of China (NSFC) Grant 81670317, 82071573 and 82271605 to Xiao-fan Wu.

Appendix A. Supplementary data

Supplementary data to this article can be found online at https://doi.org/10.1016/j.redox.2023.102763.

References

[1] P. Libby, The changing landscape of atherosclerosis, Nature 592 (2021) 524–533.
[2] Y. Kojima, I.L. Weissman, N.J. Leeper, The role of efferocytosis in atherosclerosis, Circulation 135 (2017) 476–489.
[3] E. Thorp, I. Tabas, Mechanisms and consequences of efferocytosis in advanced atherosclerosis, J. Leukoc. Biol. 86 (2009) 1089–1095.
[4] I.M. Quesada, A. Lucero, C. Amaya, D.N. Meijles, M.E. Cifuentes, P.J. Pagano, C. Castro, Selective inactivation of NADPH oxidase 2 causes regression of vascularization and the size and stability of atherosclerotic plaques, Atherosclerosis 242 (2015) 469–475.
[5] H. Hartwig, C. Silvestre-Roig, J. Hendrikse, L. Beckers, N. Paulin, K. Van der Heiden, Q. Braster, M. Drechsler, M.J. Daemen, E. Lutgens, O. Soehnlein, Atherosclerotic plaque destabilization in mice: a comparative study, PLoS One 10 (2015), e0141019.
[6] S.X. Jin, L.H. Shen, P. Nie, W. Yuan, L.H. Hu, D.D. Li, X.J. Chen, X.K. Zhang, B. He, Endogenous renovascular hypertension combined with low shear stress induces plaque rupture in apolipoprotein E-deficient mice, Arterioscler. Thromb. Vasc. Biol. 32 (2012) 2372–2379.
[7] B. Cai, E.B. Thorp, A.C. Doran, B.E. Sansbury, M.J. Daemen, B. Dorweiler, M. Spite, G. Fredman, I. Tabas, MerTK receptor cleavage promotes plaque necrosis and defective resolution in atherosclerosis, J. Clin. Invest. 127 (2017) 564–568.
[8] S. Ding, N. Lin, X. Sheng, Y. Zhao, Y. Su, L. Xu, R. Tong, Y. Yan, Y. Fu, J. He, et al., Melatonin stabilizes rupture-prone vulnerable plaques via regulating macrophage polarization in a nuclear circadian receptor RORalpha-dependent manner, J. Pineal Res. 67 (2019), e12581.
[9] G.Y. Liou, P. Storz, Detecting reactive oxygen species by immunohistochemistry, Methods Mol. Biol. 1292 (2015) 97–104.
[10] A.N. Seneviratne, A. Edsfeldt, J.E. Cole, C. Kassiteridi, M. Swart, I. Park, P. Green, T. Khoyratty, D. Saliba, M.E. Goddard, et al., Interferon regulatory factor 5 controls necrotic core formation in atherosclerotic lesions by impairing efferocytosis, Circulation 136 (2017) 1140–1154.
[11] Y. Kojima, J.P. Volkmer, K. McKenna, M. Civelek, A.J. Lusis, C.L. Miller, D. Direnzo, V. Nanda, J. Ye, A.J. Connolly, et al., CD47-blocking antibodies restore phagocytosis and prevent atherosclerosis, Nature 536 (2016) 86–90.
[12] D.M. Schrijvers, G.R. De Meyer, M.M. Kockx, A.G. Herman, W. Martinet, Phagocytosis of apoptotic cells by macrophages is impaired in atherosclerosis, Arterioscler. Thromb. Vasc. Biol. 25 (2005) 1256–1261.
[13] M.L. Brophy, Y. Dong, H. Tao, P.G. Yancey, K. Song, K. Zhang, A. Wen, H. Wu, Y. Lee, M.V. Malovichko, et al., Myeloid-specific deletion of epsins 1 and 2 reduces atherosclerosis by preventing LRP-1 downregulation, Circ. Res. 124 (2019) e6–e19.
[14] G. Sule, B.H. Abuaita, P.A. Steffes, A.T. Fernandes, S.K. Estes, C. Dobry, D. Pandian, J.E. Gudjonsson, J.M. Kahlenberg, M.X. O'Riordan, J.S. Knight, Endoplasmic reticulum stress sensor IRE1alpha propels neutrophil hyperactivity in lupus, J. Clin. Invest. 131 (2021).
[15] J.S. Knight, W. Zhao, W. Luo, V. Subramanian, A.A. O'Dell, S. Yalavarthi, J. B. Hodgin, D.T. Eitzman, P.R. Thompson, M.J. Kaplan, Peptidylarginine deiminase inhibition is immunomodulatory and vasculoprotective in murine lupus, J. Clin. Invest. 123 (2013) 2981–2993.
[16] B.C. Zhang, C.W. Zhang, C. Wang, D.F. Pan, T.D. Xu, D.Y. Li, Luteolin attenuates foam cell formation and apoptosis in ox-LDL-stimulated macrophages by enhancing autophagy, Cell. Physiol. Biochem. 39 (2016) 2065–2076.
[17] D.N. Petrusca, Y. Gu, J.J. Adamowicz, N.I. Rush, W.C. Hubbard, P.A. Smith, E. V. Berdyshev, K.G. Birukov, C.H. Lee, R.M. Tuder, et al., Sphingolipid-mediated inhibition of apoptotic cell clearance by alveolar macrophages, J. Biol. Chem. 285 (2010) 40322–40332.
[18] Y. Yang, Y. Liu, X. Chen, J. Gong, Z. Huang, W. Wang, Y. Shi, Y. Wang, J. Yao, Z. Shen, et al., 5-Aminolevulinic acid-mediated sonodynamic therapy alleviates atherosclerosis via enhancing efferocytosis and facilitating a shift in the Th1/Th2 balance toward Th2 polarization, Cell. Physiol. Biochem. 47 (2018) 83–96.
[19] H.N. Lee, Y.J. Surh, Resolvin D1-mediated NOX2 inactivation rescues macrophages undertaking efferocytosis from oxidative stress-induced apoptosis, Biochem. Pharmacol. 86 (2013) 759–769.
[20] A. Herrero-Cervera, O. Soehnlein, E. Kenne, Neutrophils in chronic inflammatory diseases, Cell. Mol. Immunol. 19 (2022) 177–191.
[21] C. Silvestre-Roig, Q. Braster, A. Ortega-Gomez, O. Soehnlein, Neutrophils as regulators of cardiovascular inflammation, Nat. Rev. Cardiol. 17 (2020) 327–340.
[22] A. Bonaventura, F. Montecucco, F. Dallegri, F. Carbone, T.F. Luscher, G.G. Camici, L. Liberale, Novel findings in neutrophil biology and their impact on cardiovascular disease, Cardiovasc. Res. 115 (2019) 1266–1285.
[23] A.C. Doran, A. Yurdagul Jr., Tabas I: efferocytosis in health and disease, Nat. Rev. Immunol. 20 (2020) 254–267.
[24] H. Tao, P.G. Yancey, V.R. Babaev, J.L. Blakemore, Y. Zhang, L. Ding, S. Fazio, M. F. Linton, Macrophage SR-BI mediates efferocytosis via Src/PI3K/Rac1 signaling and reduces atherosclerotic lesion necrosis, J. Lipid Res. 56 (2015) 1449–1460.
[25] J. Schlegel, M.J. Sambade, S. Sather, S.J. Moschos, A.C. Tan, A. Winges, D. DeRyckere, C.C. Carson, D.G. Trembath, J.J. Tentler, et al., MERTK receptor tyrosine kinase is a therapeutic target in melanoma, J. Clin. Invest. 123 (2013) 2257–2267.
[26] Y. Zhang, P. Murugesan, K. Huang, H. Cai, NADPH oxidases and oxidase crosstalk in cardiovascular diseases: novel therapeutic targets, Nat. Rev. Cardiol. 17 (2020) 170–194.
[27] U. Forstermann, N. Xia, H. Li, Roles of vascular oxidative stress and nitric oxide in the pathogenesis of atherosclerosis, Circ. Res. 120 (2017) 713–735.
[28] F. Violi, P. Pignatelli, Clinical application of NOX activity and other oxidative biomarkers in cardiovascular disease: a critical review, Antioxidants Redox Signal. 23 (2015) 514–532.
[29] F. Violi, P. Pignatelli, Platelet NOX, a novel target for anti-thrombotic treatment, Thromb. Haemostasis 111 (2014) 817–823.
[30] L. Saba, T. Saam, H.R. Jager, C. Yuan, T.S. Hatsukami, D. Saloner, B.A. Wasserman, L.H. Bonati, M. Wintermark, Imaging biomarkers of vulnerable carotid plaques for stroke risk prediction and their potential clinical implications, Lancet Neurol. 18 (2019) 559–572.

[31] C. Silvestre-Roig, M.P. de Winther, C. Weber, M.J. Daemen, E. Lutgens, O. Soehnlein, Atherosclerotic plaque destabilization: mechanisms, models, and therapeutic strategies, Circ. Res. 114 (2014) 214–226.
[32] K. Hirano, W.S. Chen, A.L. Chueng, A.A. Dunne, T. Seredenina, A. Filippova, S. Ramachandran, A. Bridges, L. Chaudry, G. Pettman, et al., Discovery of GSK2795039, a novel small molecule NADPH oxidase 2 inhibitor, Antioxidants Redox Signal. 23 (2015) 358–374.
[33] J. Reis, M. Massari, S. Marchese, M. Ceccon, F.S. Aalbers, F. Corana, S. Valente, A. Mai, F. Magnani, A. Mattevi, A closer look into NADPH oxidase inhibitors: validation and insight into their mechanism of action, Redox Biol. 32 (2020), 101466.
[34] M. Sobaniec-Lotowska, W. Sobaniec, S. Sulkowski, M. Sulik, H. Ostapiuk, [Clinico-morphologic analysis of subacute sclerosing panencephalitis in patients up to the 19th year of life], Pol. Tyg. Lek. 45 (1990) 549–552.
[35] F. Otsuka, M.C. Kramer, P. Woudstra, K. Yahagi, E. Ladich, A.V. Finn, R.J. de Winter, F.D. Kolodgie, T.N. Wight, H.R. Davis, et al., Natural progression of atherosclerosis from pathologic intimal thickening to late fibroatheroma in human coronary arteries: a pathology study, Atherosclerosis 241 (2015) 772–782.
[36] U.K. Dhawan, A. Singhal, M. Subramanian, Dead cell and debris clearance in the atherosclerotic plaque: mechanisms and therapeutic opportunities to promote inflammation resolution, Pharmacol. Res. 170 (2021), 105699.
[37] M.R. Elliott, F.B. Chekeni, P.C. Trampont, E.R. Lazarowski, A. Kadl, S.F. Walk, D. Park, R.I. Woodson, M. Ostankovich, P. Sharma, et al., Nucleotides released by apoptotic cells act as a find-me signal to promote phagocytic clearance, Nature 461 (2009) 282–286.
[38] E. Thorp, D. Cui, D.M. Schrijvers, G. Kuriakose, I. Tabas, Mertk receptor mutation reduces efferocytosis efficiency and promotes apoptotic cell accumulation and plaque necrosis in atherosclerotic lesions of apoe-/- mice, Arterioscler. Thromb. Vasc. Biol. 28 (2008) 1421–1428.
[39] H. Ait-Oufella, V. Pouresmail, T. Simon, O. Blanc-Brude, K. Kinugawa, R. Merval, G. Offenstadt, G. Leseche, P.L. Cohen, A. Tedgui, Z. Mallat, Defective mer receptor tyrosine kinase signaling in bone marrow cells promotes apoptotic cell accumulation and accelerates atherosclerosis, Arterioscler. Thromb. Vasc. Biol. 28 (2008) 1429–1431.
[40] P.G. Yancey, J. Blakemore, L. Ding, D. Fan, C.D. Overton, Y. Zhang, M.F. Linton, S. Fazio, Macrophage LRP-1 controls plaque cellularity by regulating efferocytosis and Akt activation, Arterioscler. Thromb. Vasc. Biol. 30 (2010) 787–795.
[41] E. Lutgens, M. Tjwa, P. Garcia de Frutos, E. Wijnands, L. Beckers, B. Dahlback, M. J. Daemen, P. Carmeliet, L. Moons, Genetic loss of Gas6 induces plaque stability in experimental atherosclerosis, J. Pathol. 216 (2008) 55–63.
[42] H. Ait-Oufella, K. Kinugawa, J. Zoll, T. Simon, J. Boddaert, S. Heeneman, O. Blanc-Brude, V. Barateau, S. Potteaux, R. Merval, et al., Lactadherin deficiency leads to apoptotic cell accumulation and accelerated atherosclerosis in mice, Circulation 115 (2007) 2168–2177.
[43] D. Yan, J.M. Huelse, D. Kireev, Z. Tan, L. Chen, S. Goyal, X. Wang, S.V. Frye, M. Behera, F. Schneider, et al., MERTK activation drives osimertinib resistance in EGFR-mutant non-small cell lung cancer, J. Clin. Invest. (2022) 132.
[44] P. Sen, M.A. Wallet, Z. Yi, Y. Huang, M. Henderson, C.E. Mathews, H.S. Earp, G. Matsushima, A.S. Baldwin Jr., R.M. Tisch, Apoptotic cells induce Mer tyrosine kinase-dependent blockade of NF-kappaB activation in dendritic cells, Blood 109 (2007) 653–660.
[45] E. Thorp, T. Vaisar, M. Subramanian, L. Mautner, C. Blobel, I. Tabas, Shedding of the Mer tyrosine kinase receptor is mediated by ADAM17 protein through a pathway involving reactive oxygen species, protein kinase Cdelta, and p38 mitogen-activated protein kinase (MAPK), J. Biol. Chem. 286 (2011) 33335–33344.
[46] S. Sather, K.D. Kenyon, J.B. Lefkowitz, X. Liang, B.C. Varnum, P.M. Henson, D. K. Graham, A soluble form of the Mer receptor tyrosine kinase inhibits macrophage clearance of apoptotic cells and platelet aggregation, Blood 109 (2007) 1026–1033.
[47] Y. Zhang, Y. Wang, D. Zhou, L.S. Zhang, F.X. Deng, S. Shu, L.J. Wang, Y. Wu, N. Guo, J. Zhou, Z.Y. Yuan, Angiotensin II deteriorates advanced atherosclerosis by promoting MerTK cleavage and impairing efferocytosis through the AT(1)R/ROS/p38 MAPK/ADAM17 pathway, Am. J. Physiol. Cell Physiol. 317 (2019) C776–C787.
[48] B. Cai, E.B. Thorp, A.C. Doran, M. Subramanian, B.E. Sansbury, C.S. Lin, M. Spite, G. Fredman, I. Tabas, MerTK cleavage limits proresolving mediator biosynthesis and exacerbates tissue inflammation, Proc. Natl. Acad. Sci. U. S. A. 113 (2016) 6526–6531.